

Research article

Processing effects on crystal morphology and application performance of blown films from propylene-ethylene random copolymers

Markus Zach, Davide Tranchida[✉], Enrico Carmeli[✉], Jingbo Wang, Markus Gahleitner^{*✉}, Bernhard Hofko, Elena Pomakhina, Minna Aarnio-Winterhof

Borealis Polyolefine GmbH, Innovation Headquarters, St. Peterstr. 25, 4021 Linz, Austria

Received 27 March 2024; accepted in revised form 23 April 2024

Abstract. Blown films from ethylene-propylene random copolymers (C2C3-RACOs) are used in many packaging applications today, constituting a major fraction of both mono- and multilayer packaging film constructions. Combining high processing speed and output with good mechanical and optical performance, mostly high toughness and low haze, requires understanding the structure-property-processing relations. To improve said understanding for C2C3-RACO blown films, two commercial grades with a nearly identical C2 content of ~4.4 wt% and identical melt flow rate (MFR) but different nucleation were selected. These were tested in a processing study, varying melt temperature, blow-up ratio (BUR) and neck length. The film structure was analysed by wide angle X-ray scattering (WAXS) and atomic force microscopy (AFM), and the performance by standard mechanical and optical tests. Variation of film crystallinity was found to be in the range of 62 to 65%, much smaller than in earlier cast film studies on comparable polymers. The tensile modulus is the only performance parameter for which a general positive correlation to crystallinity can be found, blown films being about 50% stiffer than the softest cast films of a comparable polymer. Ductility and toughness are enhanced by higher orientation, resulting from higher BUR and/or higher neck length. For transparency and haze, low surface roughness is decisive at comparable crystallinity, which can be achieved by increasing melt temperature.

Keywords: polyolefins, film, extrusion, nucleation agent, crystallinity

1. Introduction

Blown film extrusion is a very economical polymer conversion process, allowing the production of mono- and multilayer films in the thickness range of about 20 to 200 μm with only limited orientation [1]. In general, during processing the molecular characteristics of the polymer couple with the processing conditions to determine structure and morphology and, thus, the performance of the film [2, 3]. Therefore, the understanding of structure-property-processing relations (SPPR) is fundamental to control and optimize the process and the end-use properties of the product.

Film blowing is a standard technique for polyethylene (PE) processing since the early days of high-pressure process based low density PE (LDPE), having later been expanded to low-pressure products high density PE (HDPE) and linear low density PE (LLDPE) as well as blends based on these classes. Thus, extensive work on SPPR has been reported for PE blown films, with blow-up ratio (BUR) and take-up ratio (TUR) being the two most impactful parameters. On the one hand, the BUR is used to control the film thickness, which in turn determines the cooling rate gradient across the film. This strongly affects the total crystallinity and the spatial evolution of the

*Corresponding author, e-mail: markus.gahleitner@borealisgroup.com
© BME-PT

lamellar thickness. On the other hand, the TUR determines the stresses that occur in machine direction, and thus dominates the orientation [4, 5]. Several studies aimed at explaining the differences of tear strength in machine (MD) or in transverse direction (TD) for PE with different densities and microstructures [6–8]. In general, the large differences in tear performance must be ascribed to the crystalline lamellar structure rather than to the orientation of the amorphous phase.

For HDPE and LDPE blown films, fibrillar structures are found in MD, and they are responsible for the formation of row nuclei, which cause higher tensile strength in MD over TD [6]. For LLDPE, Zhang *et al.* [6] found a more balanced tear strength which they related to a lower overall orientation and a spherulite-like superstructure. Krishnaswamy and Sukhadia [9] found that higher or lower MD extension rates (*i.e.* higher or lower TUR) in LLDPE result in higher tear strength in TD or in MD, respectively. This research group also tried to explain the morphological origin of the Elmendorf tear resistance: (i) tear resistance in MD is dominated by the shear deformation occurring between lamellae via crystallographic slip. (ii) Instead, chain pull-out along the lamellar long axis that is aligned in TD is responsible for the tear resistance in TD. Other studies focused on understanding the relation between surface roughness or optics of the films to polymer design and processing conditions [10–13]. Blown films produced with a Ziegler-Natta catalyst (ZN) showed a higher degree of orientation compared to films made of metallocene catalyzed PE, related to the intrinsically narrower molecular weight distribution of metallocene PEs, and therefore the lack of long chains and the shorter relaxation times when compared to ZN-PEs. Moreover, in ZN-PE films the higher orientation leads to rod-like structures at the film surface that determine a higher haze [10, 12]. A similar conclusion was found by Zhao *et al.* [13] for PEs with different types of olefin copolymers. In general, the observed final film morphology is likely due to consolidation of the initial chain orientation (caused by the applied stresses) through the crystallization process [4]. Crystallization can continue also above the frost line, where the bubble changes no longer shape [5, 14]. Thus, varying the cooling rate, *i.e.*, BUR, can be a tool to control surface roughness and optics of the final film [11].

Differently to PE, the number of studies on SPPR for polypropylene (PP) blown films is rather limited. This might be due to the intrinsically lower melt strength [15] and bubble stability of PP when compared to PE. In this regard, some investigations focused on the use of high melt strength (HMS) PP in the blown film application [16–19]. In the work of Chang *et al.* [19], blown films of HMS PP showed the formation of stacks of lamellae oriented in TD, *i.e.* edge-on. This morphology was observed all across the film thickness, although longer lamellae were detected in the core of the film, likely due to the lower cooling rate experienced by the chains in the core compared to the chains near the film surface. Moreover, a row nucleated structure developed along MD was deduced from 2D-wide angle X-ray scattering (WAXS) patterns. Row-nuclei are also usually seen when orientation in the melt is applied to HDPE [7], and the formation of extended chain fibrillar crystals (shish) can serve as nucleation sites for lamellae that are growing perpendicularly to the extended chains (kebab). In the case of HMS PP, the high molecular weight chains, that are responsible for the higher melt strength [20], have a longer relaxation time and thus remain oriented until crystallization occurs. Those oriented chains are the precursors of row-nuclei. In PP homopolymer blown films, strong orientation in MD was observed, which causes a highly anisotropic mechanical behavior [21]. Differently, no specific orientation of the crystals was reported for a blown film of propylene-ethylene random copolymer [22]. In general, findings on the bulk structure are relevant to explain the final mechanical properties of the blown films. Instead, for optical performance a major role is played by surface properties. Indeed, as shown in an early paper by Bheda and Spruiell [23], the transmission of light through PP blown films is strongly correlated with the surface roughness, which is more affected by the crystallization process at the film surface than by the rheological behavior of the polymer.

Polymorphism should also be considered when dealing with SPPR of PP, which can crystallize under different phases. From an industrial perspective, the most relevant ones are monoclinic (α), trigonal (β), and orthorhombic (γ) forms [24]. Moreover, a metastable structure, called mesophase, with a degree of order intermediate between crystalline and amorphous phase can also be obtained via fast cooling

from the melt [25]. In the application area of films, the effect of processing parameters on the formation of specific crystalline phases of PP was thoroughly studied for cast films [26, 27], even with *in-situ* structural measurements [28]. The general conclusion is that the chill-roll temperature is the parameter causing crucial effects for the final crystalline structure. For blown films, reports in the literature are lacking. Some aspects of polymorphism induced on a PP homopolymer were reported by Savolainen, using a process for producing bi-axial oriented PP (BOPP) via a specific blown film process [29]. He observed that the mesophase structure formed by quenching the melt exiting the die with a cooling mandrel is then transformed into stable α -crystals via re-heating and drawing of the film during the bubble forming process.

Products based on pure PP are intrinsically stiffer than PE products. For this reason, some investigations focused on the addition of PP to LLDPE or addition of LLDPE to PP for blown film application, either via blending or multilayer structure, with the aim of increasing mechanical strength or toughness of the final film, respectively [17, 19, 21, 22]. LLDPE shows a certain compatibility in the melt state with PP, contrarily to other PE types [30, 31]. Zhang and Ajji [22] reported that the orientation of crystals of LLDPE is different in multilayer films with PP compared to films from LLDPE/PP blends. In contrast to that, the orientation in the PP phase is the same in the multilayer as in the blend film. The orientation of LLDPE crystals in the blend film towards the thickness direction was explained via the occurrence of epitaxial growth on top of the already formed PP crystals during cooling from the melt, based on the well-known epitaxial relationship between the two polymers [32]. In the multilayer film, only a thin epitaxial LLDPE layer was observed at the interface with the PP layer. These findings agree with the investigation of Chang *et al.* [19], who studied blown films made from LLDPE blended with up to 30 wt% HMS PP. They observed strongly elongated domains of HMS PP in MD due to the shear forces applied during the formation of the bubble. This elongated shape is retained in the melt due to the high melt strength of HMS PP, which prevents the dispersed domains to break up into smaller droplets. In turn, the PP chains are also elongated and form lamellae oriented in TD. Eventually, those HMS PP lamellae act as row nuclei on which the LLDPE lamellae

grow epitaxially. The observed crystalline structures in the blend film caused a reinforcement of the mechanical performance of LLDPE in MD, that was proportional to the HMS PP concentration. On the other hand, the stress-strain behavior remained almost unaltered in TD. In blown films made of blends with majority homopolymer PP and minority LLDPE or very low-density PE (VLDPE), Silva *et al.* [21] found that the PP crystalline phase has a lamellar structure with no dominant orientation rather than shish-kebabs, eventually resulting in more balanced tensile properties in MD and TD.

Given the lack of studies for PP in the area of blown film, the present investigation aims at increasing the understanding of processing effects on crystalline structure, surface quality and final mechanical and optical performance for propylene-ethylene random copolymer (C2C3-RACO) blown films, which by far dominate this application segment.

2. Experimental work

Two commercial α -nucleated C2C3-RACOs of Borealis AG (Austria) were selected for this study, the key parameters of which are summarized in Table 1. Both are based on a post-phthalate ZN catalyst [33, 34], have identical melt flow rate (MFR) as measured according to ISO 1133 at 230 °C and 2.16 kg load of 1.5 g/10 min. The grades also have a similar ethylene content, but differ in dispersity and nucleation. PPR-A is designed for blown film applications using a particulate nucleating agent of organophosphate-type (hydroxybis-(2,4,8,10-tetra-tert-butyl-6-hydroxy-12h-dibenzo-(d,g)(1,3,2)-dioxaphosphocin-oxidato)-aluminium, commercially available as ADK STAB NA-21E from Asahi Denka Kogyo, Japan), while PPR-B is a blow molding type with a soluble nucleating agent from the sorbitol class (clarifier, 1,2,3,4-bis(3,4-dimethyl-benzidilene sorbitol, commercially available as Millad 3988 from Milliken Inc., USA). Nucleation has been found to be instrumental in achieving process stability in air-cooled PP film blowing as viable alternative to the originally used addition of long-chain branched HMS-PP [16–20]. Both nucleating agent types are used at concentrations suitable to achieve good transparency [35].

Differential scanning calorimetry (DSC) analysis was run according to ISO 11357, determining the melting peak temperature (T_m) and melting enthalpy (H_m) as well as the crystallization peak temperature

Table 1. Basic data of used PP copolymers.

	Rheology 200 °C			DSC				NMR	XCS	WAXS film	
	η_0 [Pa·s]	ω_c [rad/s]	$10^5/G_c$ [°C]	T_m [°C]	H_m [J/g]	X_c [%]	T_c [°C]	C2 total [wt%]	ISO [wt%]	X_c [%]	K_γ [%]
PPR-A	25980	10	3.38	147.3	82.0	39.2	117.8	4.3	7.5	63.3	9
PPR-B	20980	12	3.43	146.4	78.6	37.6	115.7	4.4	8.9	62.6	11

Basic data of used PP copolymers (data from blown film at extrusion temperature 210 °C, BUR 2.5, TUR 12 and normal neck length).

(T_c) with a TA Instruments (USA) Q200 differential scanning calorimeter on 5 mg samples. DSC was run in a heat/cool/heat cycle with a scan rate of 10 °C/min in the temperature range of –30 to +225 °C. Only one crystallization temperature (T_c) was observed and determined from the cooling step, while the melting temperatures (T_m) and the overall melting enthalpy (H_m) were determined from the second heating step. The total C2 content was measured by ^{13}C nuclear magnetic resonance (NMR) spectroscopy, using a Bruker (USA) Avance III 400 NMR spectrometer operating at 400.15 and 100.62 MHz for ^1H and ^{13}C respectively. The spectra were recorded at 125 °C on polymer dissolved in 7,2-tetrachloroethane-*cf*2 (TCE-*cf*2) along with chromium (III) acetylacetonate ($\text{Cr}(\text{acac})_3$) as relaxation agent. Signal assignment and evaluation was performed according to Wang and Zhu [36].

The melt rheological measurements of storage and loss moduli G' , $G''(\omega)$ were carried out according to ISO 6721-1, using an Anton Paar (Austria) MCR 301 Rheometer equipped with a convection oven. The measurements were performed under nitrogen atmosphere to prevent oxidation and degradation. Parallel plate-plate geometry was used, with plates 25 mm in diameter. The frequency range was from 0.01 to 628 rad/s with five points per decade. The applied strain was from 2 to 7%, well below the previously determined linearity limit of 15%, and the gap between the plates 1.3 mm. The polydispersity index (PI), was calculated from the crossover point, located at the crossover frequency ω_c at which storage and loss modulus curves intersect (Equation (1)):

$$G_c = G'(\omega_c) = G''(\omega_c) \quad (1)$$

PI is then defined as the inverse of the crossover modulus G_c with a pre-factor of 10^5 to achieve a simple figure [37, 38] (Equation (2)):

$$PI = \frac{10^5}{G_c} \quad (2)$$

The zero shear viscosity (η_0) was determined from the complex viscosity $\eta^*(\omega)$ assuming validity of the Cox-Merz relation [39, 40].

The films were prepared using a monolayer blown film lab line manufactured by Collin Lab & Pilot Solutions (Germany). The line is equipped with a 30 mm 3-zone single screw extruder in a length of 30/LD. A filter package in a mesh size of 400/900/400 mesh per cm^2 was used. The spiral distributor blow head is equipped with a 50 mm (HDPE set-up) or 60 mm (PP and LDPE set-up) die and a die-gap of 1.5 mm. To cool down the film, an active cooled standard duo-lip cooling ring with 13 °C cooling air was used. The bubble was stabilised by a roller calibration basket and hardwood strips collapsing unit. The width of the film is automatically controlled according to the defined blow-up ratio (BUR) and finally wound on 3 inch cores in a contact winder.

A detailed study of PPR-A and a single reference point for PPR-B was realised (the latter being based on the fact that this grade is considered less suitable for film blowing), for which blown films of 50 μm thickness were produced under different process conditions. Different blow-up ratios (BUR) of 1:2, 1:2.5 and 1:3 were defined. The extruder temperature varied between 210 and 240 °C. Finally, the neck length was changed between “short neck” (PP set-up with 60 mm die-diameter) and “long neck” (HDPE set-up with 50 mm die-diameter) with frost line high of 5D.

The output was fixed to 8 kg/h, resulting in a reduction of take-up ratio (TUR) with increasing BUR. Furthermore, the die-gap remained to 1.5 mm and the film thickness was kept at 50 μm . The second material, PPR-B, was used as reference and processed in standard PP blown film conditions. This means a BUR of 1:2.5, an extrusion temperature of 210 °C and a short neck set-up. Film nomenclature is summarized in Table 2.

The degree of crystallinity and the orientation of the film samples was studied by carrying out WAXS measurements in reflection mode with a Bruker

Table 2. Film nomenclature and production parameters (output and die-gap fixed at 8 kg/h and 1.5 mm).

Film T/BUR/neck	Polymer	Extrusion temperature [°C]	Blow-up ratio 1:x	Take-up ratio 1:x	Neck length [–]
A210/2.0/norm	PPR-A	210	2.0	15	normal
A210/2.5/norm	PPR-A	210	2.5	12	normal
A210/3.0/norm	PPR-A	210	3.0	10	normal
A240/2.5/norm	PPR-A	240	2.5	12	normal
A210/2.5/long	PPR-A	210	2.5	12	long
B210/2.5/norm	PPR-B	210	2.5	12	normal

Discover D8 diffractometer (Bruker Corporation, USA) equipped with a two-dimensional GADDS detector and a Ni-filtered Cu K_{α} X-rays. Three measurements were performed on each sample and the corresponding results were averaged. The amorphous halo obtained from an atactic-PP sample [41] was properly scaled and subtracted and a crystallinity index (X_c) was quantified according to (Equation (3)):

$$X_c = \frac{A_c}{A_{\text{tot}}} \quad (3)$$

where A_{tot} is the area under the total pattern and A_c is the area after subtraction of the amorphous halo. The relative content of the γ -modification was calculated using the method developed by Pae [42], also used by several other groups in similar context [43–45] (Equation (4)):

$$K_{\gamma} = \frac{I_{\gamma}(117)}{I_{\alpha}(110) + I_{\gamma}(117)} \quad (4)$$

Using the fact that the WAXD pattern of unoriented, standard isotactic PP (iPP) shows diffractions from the (110) and (040) crystallographic planes that are roughly equal in size [46], an orientation parameter (O_p) was derived, according to (Equation (5)):

$$O_p = \frac{I_{\alpha}(040)}{I_{\alpha}(110)} \quad (5)$$

where $I_{\alpha}(110)$ is the intensity of α -phase (110) and $I_{\alpha}(040)$ is the intensity of α -phase (040) reflections respectively. This ratio is close to 1 in case of an unoriented parameter, while it increases noticeably with orientation of the crystalline phase in the films, since an oriented crystalline structure scatters more or less intensely from certain crystallographic planes, as seen for the extreme case of biaxially oriented films [47].

Selected films were additionally characterized by atomic force microscopy (AFM) directly on the film

surface in order to determine structure and surface roughness of both sides (inside and outside). AFM images were collected with an Oxford Instruments (USA) MFP-3D operated in alternated contact mode and equipped with cantilevers AC160TS from Olympus using an image resolution of 1024×1024 pixels². As the films did not show any obvious inhomogeneities, only one image per film, side and magnification was taken. Absolute roughness (R_a), was calculated from Z-sensor images with size $40 \times 40 \mu\text{m}^2$ in the instrument software. The images were fitted with a plane prior to the calculation, to remove the tilt of the sample mounting. Micrographs reported in the following were obtained with Scanning Probe Image Processor (SPIP) software. All films were found to be rather smooth, with crystalline domains being separated by depressions as shown in Figure 1. The inside is always significantly smoother, reflecting the different cooling history and being in line with results from LLDPE [10].

In addition, all films were subjected to a standard characterization regime for mechanical and optical performance after at least 96 h storage at standard conditions (23 °C, 50% relative humidity). In accordance with the standards, 12 specimens per sample were tested and the average calculated from 10 excluding the highest and lowest result. This results in a standard deviation of less than 5% for modulus and optical data, and less than 10% for strain at break and toughness resp. impact data.

Tensile tests in machine (MD) and transverse direction (TD) were performed according to ISO 527-3 at 23 °C on the films as produced indicated below. Testing was performed at a cross head speed of 1 mm/min for modulus determination and at 10 mm/min beyond until fracture. The dart drop impact strength (DDI) was measured according to ISO 7765-1:1988/Method A from the films. This test method covers the determination of the energy that causes films to fail under specified conditions of

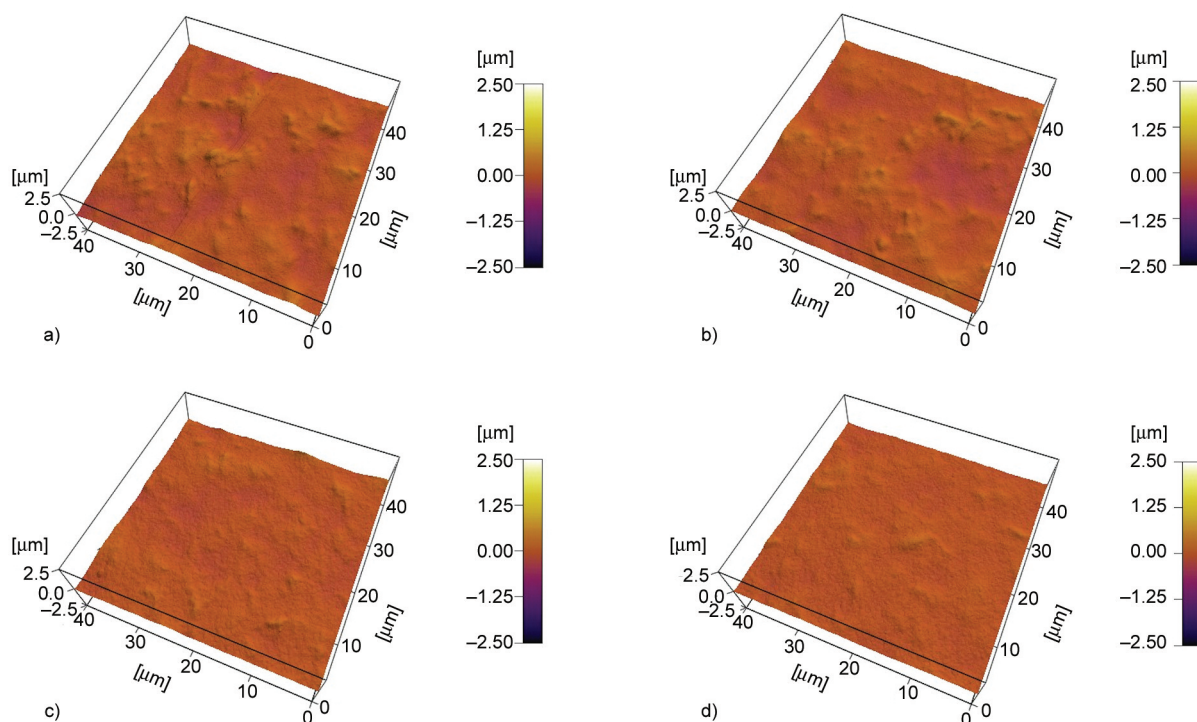


Figure 1. AFM-based surface profile images for films from PPR-A: a) A210/2.5/norm outside, b) A210/2.5/norm inside, c) A240/2.5/norm outside, d) A240/2.5/norm inside.

impact of a free-falling dart from a specified height that would result in failure of 50% of the specimens tested (Staircase method A). A uniform dart mass increment is employed during the test, and the missile weight is decreased or increased by the uniform increment after test of each specimen, depending upon the result (failure or no failure) observed for the specimen. Elmendorf tear resistance was performed in MD and TD, measuring tear strength according to ISO 6383/2. This is the force required to propagate tearing across a film sample, measured using a pendulum device and normalized by the film thickness. Gloss was measured according to ASTM D2457 at 20° in MD and TD. Transmittance, haze and clarity were determined according to ASTM D 1003-00, but no transmittance data will be reported because these were all in the range of ~93%.

3. Results and discussion

Although there are several studies dealing with the effect of processing parameters on structure (crystallinity) and performance (mechanics and optics) of PP cast films (CF), the number of respective papers dealing with blown films is rather limited [16–23]. The primary objective was therefore to understand to which extent a variation inside the limits of stable operation can affect these. An important aspect was

anisotropy, as both cast and blown films are normally considered unoriented, in order to distinguish them from mono- or biaxially oriented films [47]. We therefore calculated mechanical orientation parameters from properties measured in MD and TD, namely for the tensile modulus (Equation (6)):

$$AI_{TM} = \frac{TM(MD)}{TM(TD)} \quad (6)$$

for the strain at break (*StrB*) (Equation (7)):

$$AI_{StrB} = \frac{StrB(MD)}{StrB(TD)} \quad (7)$$

and for the Elmendorf tear resistance (*ETR*) (Equation (8)):

$$AI_{ETR} = \frac{ETR(MD)}{ETR(TD)} \quad (8)$$

to be included in the evaluation. Moreover, the results were compared to those of another C2C3-RACO used in a recent CF study [26].

In Table 3, an overview of the WAXS and tensile test is assembled. One notes that crystallinity variation is limited and the γ -modification content much lower than in typical morphologies developed in DSC experiments, as to be expected at the rather high cooling rate in film blowing [26, 34]. Only the film based

Table 3. Film crystallinity and tensile performance.

Film T/BUR/neck	WAXS			Tensile MD		Tensile TD	
	X_c [%]	K_γ [-]	Orientation [-]	Modulus [MPa]	$StrB^*$ [%]	Modulus [MPa]	$StrB^*$ [%]
A210/2.0/norm	63.4	0.11	3.62	1047	564	1003	595
A210/2.5/norm	63.3	0.09	2.90	1070	551	1035	632
A210/3.0/norm	63.2	0.09	6.85	1000	502	1033	565
A240/2.5/norm	64.7	0.11	3.25	1059	577	995	668
A210/2.5/long	63.9	0.10	2.63	1056	582	1005	492
B210/2.5/norm	62.2	0.11	2.16	964	607	969	680

**StrB*: strain at break

on PPR-B has a somewhat lower crystallinity, corresponding to a lower modulus level. This likely results from a reduced activity of the soluble nucleating agent at high cooling rates, a phenomenon observed before in high-speed calorimetry [2, 34]. Variations of crystallinity and tensile strength as caused by changes in melt temperature are presented in Figure 2a, showing that also here – as for modulus – the MD values are always higher. When increasing the BUR) at given extrusion (melt) temperature, modulus and crystallinity stay rather constant, but crystalline orientation and tensile strength increase, the latter more significantly in MD. Such increasing

anisotropy in tensile strength has been observed for LLDPE and LDPE as well [6], although there as function of draw-down ratio (corresponding to TUR in the present case) at constant BUR.

Table 4 assembles the toughness-related parameters, *ETR* and *DDI*, in combination with surface roughness and optics. Compared to ductility, an inverse relation, with TD values being always higher than MD, is observed for the *ETR*, which is an important parameter regarding opening behaviour for packaging applications [48]. While the MD-value remains rather constant, processing variations affect the TD-value, although in a rather complex way with a maximum at

Table 4. Toughness parameters, AFM-based surface roughness and optical film performance.

Film T/BUR/neck	Elmendorf tear resistance		<i>DDI</i>	AFM roughness			Gloss 45°		Optics	
	MD [N/mm]	TD [N/mm]	Method A [g]	$R_{a,inside}$ [nm]	$R_{a,outside}$ [nm]	$R_{a,total}$ [nm]	MD [%]	TD [%]	Haze [%]	Clarity [%]
A210/2.0/norm	2.9	12.7	56	–	–	–	26	25	25.4	65.7
A210/2.5/norm	4.1	28.3	59	73	106	179	26	26	24.6	69.0
A210/3.0/norm	3.5	9.4	64	–	–	–	26	26	24.3	70.8
A240/2.5/norm	3.5	8.9	71	36	50	86	56	57	9.1	92.1
A210/2.5/long	2.2	10.2	71	62	88	150	24	23	24.0	77.6
B210/2.5/norm	3.3	11.9	69	80	79	159	36	35	17.9	78.9

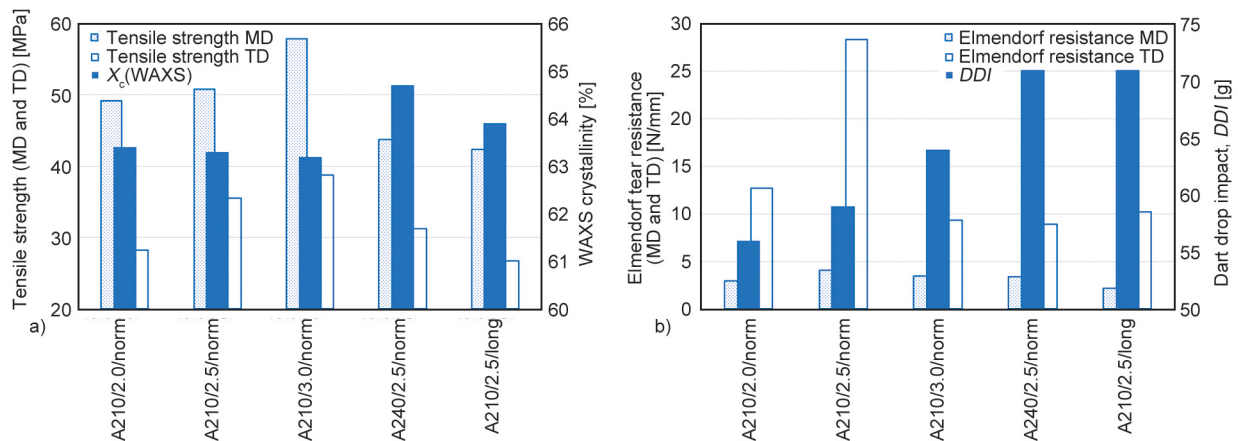


Figure 2. Processing parameter effects on a) film crystallinity and tensile strength, and b) Elmendorf resistance and *DDI* for PPR-A.

BUR of 2.5 (see Figure 2b). Complex effects on ETR have, however, also been observed for LLDPE before [9], where a positive effect of crystal orientation on $ETR(MD)$ was observed together with a negative one on $ETR(TD)$. Clearer is the effect on dart drop impact (DDI , same Figure 2b), but also here both higher crystal orientation at 210 °C and normal neck length (*i.e.* frost-line height) and higher temperature or neck length give better toughness. This is at least partly in line with earlier results for HDPE [49], where an increase in blow-up ratio was found to improve DDI .

A more complete picture is obtained when directly correlating crystallinity parameters and mechanics for both polymers together, as done in Figure 3. Rather clear is the positive effect of X_c on modulus, especially when considering the single point of PPR-B, but less clear is the effect on strain at break (a common measure for the ductility, *i.e.* the resistance to failure at slow deformation). Strain at break in TD is higher than in MD over the whole range for normal neck length, with an inverted relation only for higher neck length. The fact that this can be maintained at a high level, also without major changes in anisotropy (<20% deviation in all cases) is very relevant for blown films, which are commonly valued for their higher toughness in comparison to CF [26, 34]. When relating said anisotropy as well as the dart impact to O_p , the crystalline orientation parameter from WAXS, it becomes obvious that lower orientation is rather positive for both (see Figure 3b). This is again rather similar to the earlier findings for LLDPE [9], although in that study a difference in orientation was mostly achieved by varying the polymer structure.

All results of the optical characterizations, in combination with the surface roughness data from AFM, are summarized in Table 4. Variations in optical performance are far more limited than in the recent CF studies [26, 50, 51], and especially gloss is only changed significantly when increasing the melt temperature or when changing the polymer. In both cases a parallel reduction of haze is obvious, but while the latter change from PPR-A to PPR-B involves a crystallinity reduction, this change is opposite (from 63.3 to 64.7%) for the temperature increase. This decoupling of film crystallinity and haze is known, however, both from PP CF studies [50] and also from LLDPE BF [10]. At low haze levels of thin films, surface effects become dominant, and higher melt temperature can result in a smoother film surface, at least in absence of disturbances from processing aids like slip or anti-blocking additives.

For predominantly mesomorphic PP CF, some negative effects on haze from isolated or row-like spherulitic structures have been observed [50, 51], which are getting stronger at higher line speed. Crystallinity is, however, generally higher for the now studied blown films, and the surface structure largely consists of “blocks” of lamellar arrangements as shown in Figure 4, partly also forming a spherulitic superstructure dominating surface roughness. In addition, the higher resolution images clearly show individual lamellae. Due to convolution of tip shape, the apparent size is relatively larger than expected. However a repeating distance in the order of 30 nm can be observed, which coupled with the information of ca. 60% degree of crystallinity implies a lamellar thickness in the order of 20 nm. A comparison to earlier CF images [51] shows some similarity to films

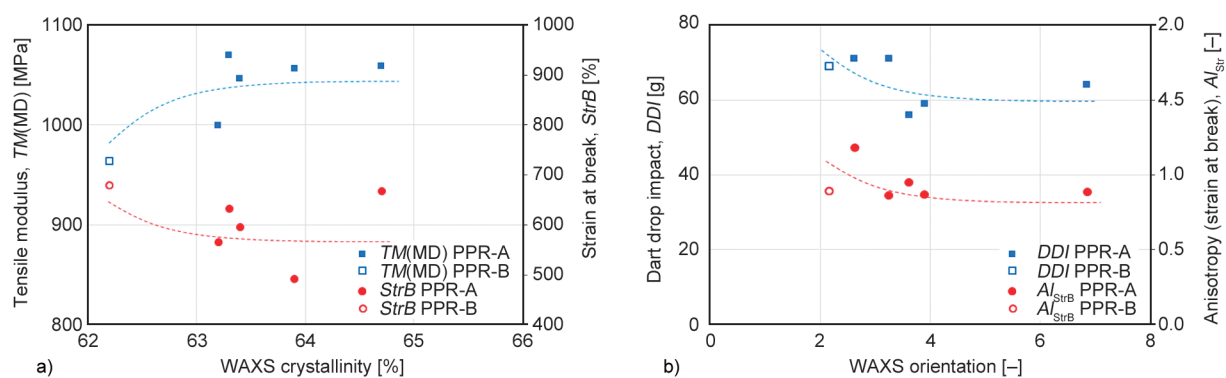


Figure 3. Correlation between a) crystallinity, MD modulus and strain at break ($StrB$), and b) orientation factor, dart drop impact strength (DDI) and anisotropy in strain at break ($A_{I_{StrB}}$) for both polymers (dashed lines are used as guide for the eye only).

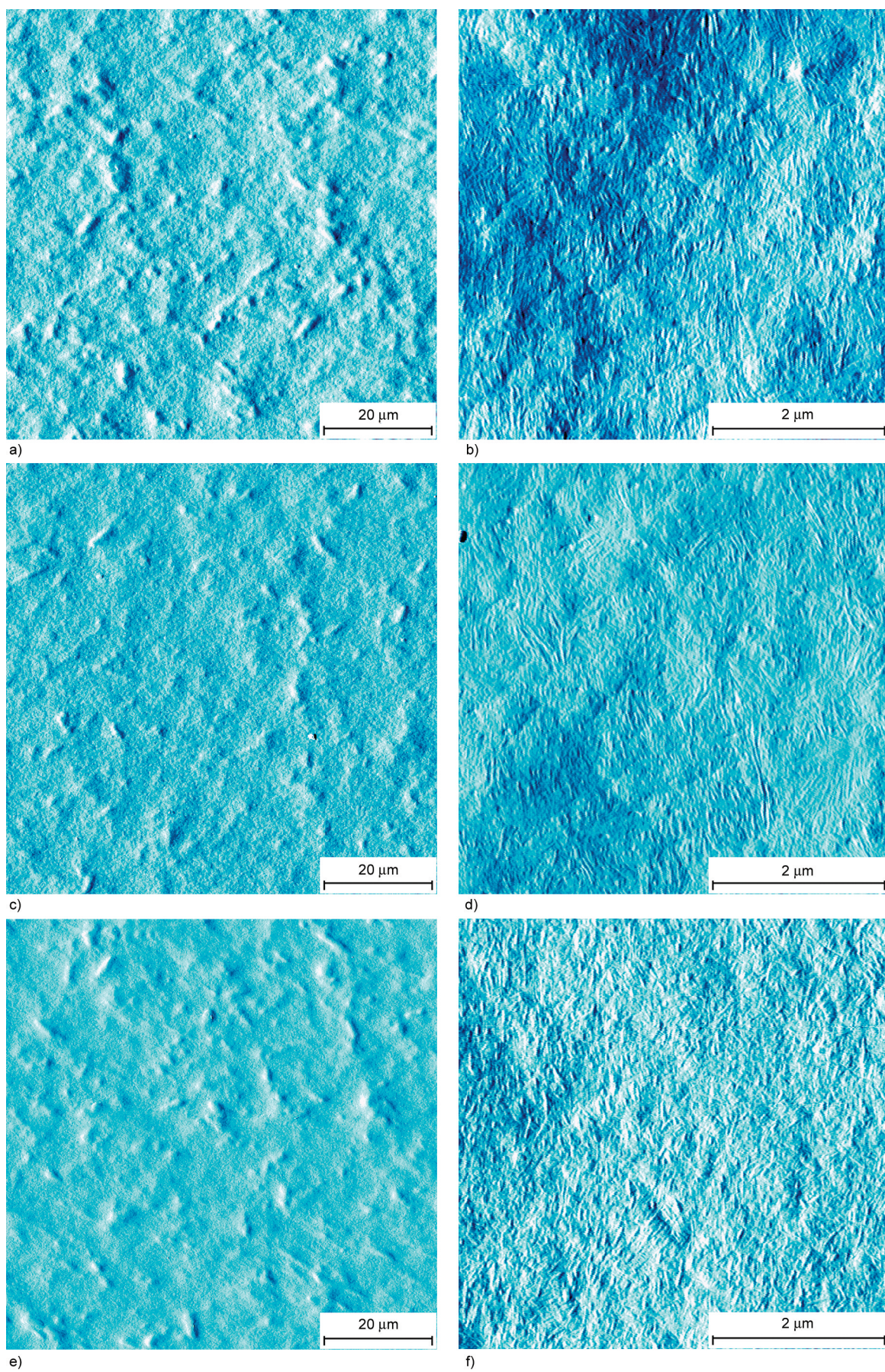


Figure 4. AFM amplitude images for outsides of films: a) and b) A210/2.5/norm, c) and d) A240/2.5/norm, e) and f) B210/2.5/norm.

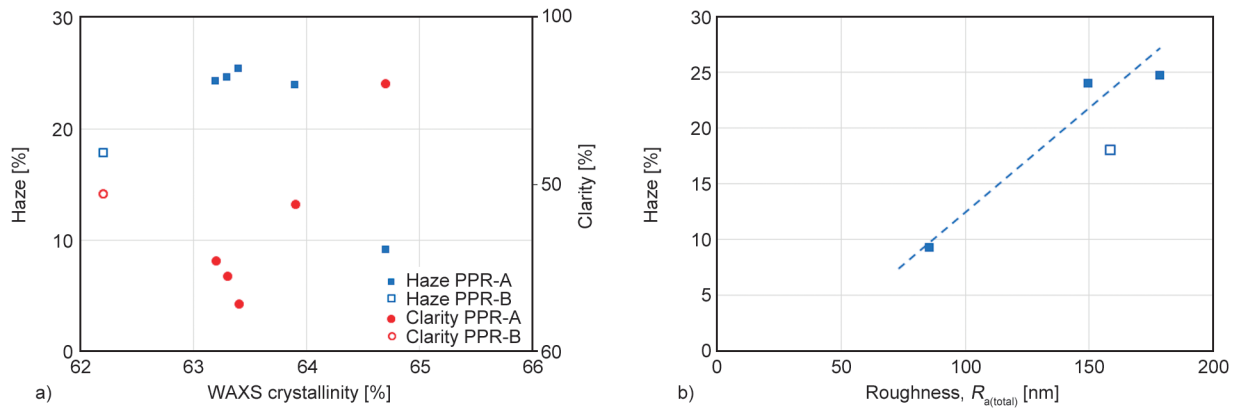


Figure 5. Correlation between a) crystallinity, haze and clarity and b) surface roughness and haze for both polymers (full symbols PPR-A, open symbols PPR-B).

produced at rather high chill roll temperature, corresponding also in terms of crystallinity.

Considering the optical data from both polymers in relation to WAXS results as in Figure 5a, one finds that within the PPR-A series films get more transparent in both close contact (haze) and distance (clarity) with increasing crystallinity. Another look at Figure 5b relating haze to surface roughness from AFM fills in the missing information: Surface roughness is clearly decisive for the three PPR-A films of comparable crystallinity, while the PPR-B film is more transparent at comparable roughness due to its lower crystallinity.

Finally, the data of PPR-A from the present study were combined with cast film (CF) results based on a wide variation of processing parameters. These are based on a PPR with a lower C2 content of 2.2 wt% and higher MFR of 8 g/10 min, as typical for that technology [26]. As Figure 6 shows, a much wider range of crystallinity can be covered in that technology, resulting from the high cooling rates achieved at low chill-roll temperatures [27, 28]. A

level of X_c above 60% as observed for the blown PPR films in the present study – and even with a higher C2 content, which is negative for crystallinity [33] – seems to be not possible. This level was only reached for PP homopolymers in the cited CF study. Variations of tensile modulus at higher crystallinity, especially in MD, were observed in cast films as well and mostly found to be resulting from changes in processing speed [2]. The orientation-based variations of the present study thus fit into the overall picture and do not disturb the general trend of Figure 6a, where the dashed line is the correlation for the CF data with a correlation coefficient R^2 of 0.988.

The situation is quite different for haze (see Figure 6b), where the variation between ~10 and ~5% at high crystallinity is in line with CF results, but the lack of a general trend clearly results from the surface roughness effects discussed above, the variation in haze at comparable crystallinity being similar for both types of polymers and films (here also the pure CF correlation reaches only R^2 of 0.841).

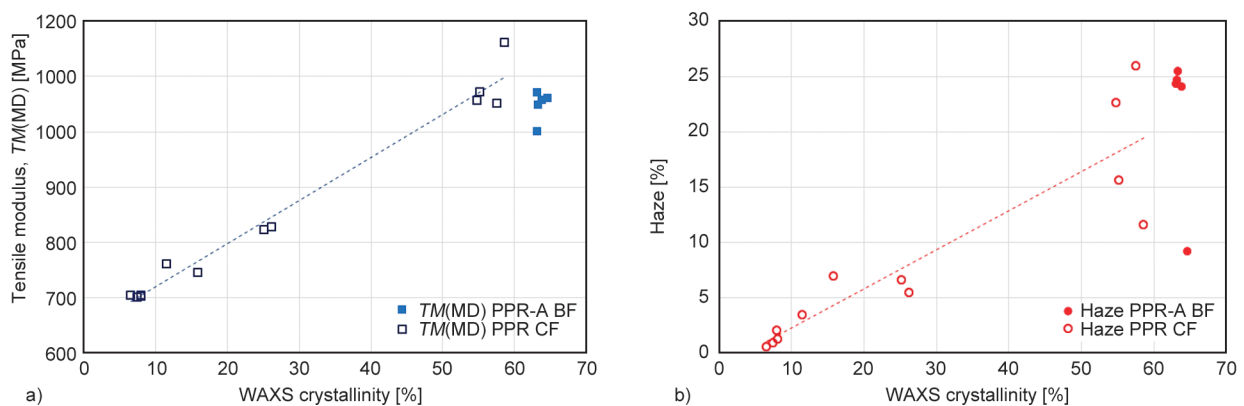


Figure 6. Correlation between a) crystallinity and modulus and b) crystallinity and haze for CF from the PPR of [26] and BF of PPR-A.

4. Conclusions

There is a clear trend today for both reducing film thickness and substituting multi-material combinations in packaging films, in order to reduce carbon footprint and enable circularity. Monolayer blown films from C2C3-RACOs are a good candidate for this due to their combination of mechanical stability, optical quality and temperature resistance. They are consequently used in many packaging applications today, constituting a major fraction of both mono- and multilayer packaging films.

The present study was aimed at improving the understanding of SPPR for this combination of polymer and application, which has received only limited attention so far. Results should enable combining high processing speed and output with good mechanical and optical performance (mostly high toughness and low haze). For the two selected commercial C2C3-RACO grades, interesting correlations between nucleation type, processing parameters, film structure and performance could be found.

The variation in film crystallinity of 62 to 65% is much smaller than in the case of cast films [26, 27], and only increased significantly by a higher melt temperature for the PPR-A (containing a particulate nucleating agent of organophosphate-type) used in the parameter variation study. The lower crystallinity of the PPR-B blown film at identical conditions likely results from a reduced activity of the soluble nucleating agent (sorbitol type) at high cooling rates [2, 34]. Variations in crystalline orientation are stronger and connected to BUR and neck length. Of all performance parameters, the tensile modulus is the only performance parameter for which a general positive correlation to crystallinity can be found, and blown films are about 50% stiffer than the softest cast films of a comparable polymer. Ductility and toughness are positively affected by higher orientation, with similar relations as observed for LLDPE [9] and HDPE [49] likewise. For gloss, transparency and haze, surface roughness is decisive at comparable crystallinity, and this can mostly be improved by raising the melt temperature.

References

- [1] Jeremic D.: Polyethylene. in ‘Ullmann's encyclopedia of industrial chemistry’ (eds.: Ley C., Elves B.) Wiley, Weinheim, 1–34 (2014).
https://doi.org/10.1002/14356007.a21_487.pub3
- [2] Mileva D., Tranchida D., Gahleitner M.: Designing polymer crystallinity: An industrial perspective. *Polymer Crystallization*, **1**, e10009 (2018).
<https://doi.org/10.1002/pcr2.10009>
- [3] Ryan A. J., Bras W., Hermida-Merino D., Cavallo D.: The interaction between fundamental and industrial research and experimental developments in the field of polymer crystallization. *Journal of Non-Crystalline Solids*, **451**, 168–178 (2016).
<https://doi.org/10.1016/j.jnoncrysol.2016.07.039>
- [4] Cherukupalli S. S., Gottlieb S. E., Ogale A. A.: Real-time Raman spectroscopic measurement of crystallization kinetics and its effect on the morphology and properties of polyolefin blown films. *Journal of Applied Polymer Science*, **98**, 1740–1747 (2005).
<https://doi.org/10.1002/app.22357>
- [5] Morris B. A.: Effect of process on properties. in ‘The science and technology of flexible packaging: Multi-layer films from resin and process to end use’ (ed.: Morris B. A.) Elsevier, Amsterdam, 575–597 (2022).
<https://doi.org/10.1016/B978-0-323-24273-8.00014-9>
- [6] Zhang X., Elkoun S., Ajji A., Huneault M.: Oriented structure and anisotropy properties of polymer blown films: HDPE, LLDPE and LDPE. *Polymer*, **45**, 217–229 (2004).
<https://doi.org/10.1016/j.polymer.2003.10.057>
- [7] Keller A., Machin M.: Oriented crystallization in polymers. *Journal of Macromolecular Science Part B: Physics*, **1**, 41–91 (1967).
<https://doi.org/10.1080/00222346708212739>
- [8] Holmes D., Miller R., Palmer R., Bunn C.: Crossed amorphous and crystalline chain orientation in polyethylene film. *Nature*, **171**, 1104–1106 (1953).
<https://doi.org/10.1038/1711104b0>
- [9] Krishnaswamy R., Sukhadia A.: Orientation characteristics of LLDPE blown films and their implications on Elmendorf tear performance. *Polymer*, **41**, 9205–9217 (2000).
[https://doi.org/10.1016/S0032-3861\(00\)00136-1](https://doi.org/10.1016/S0032-3861(00)00136-1)
- [10] Bafna A., Beaucage G., Mirabella F., Skillas G., Sukumaran S.: Optical properties and orientation in polyethylene blown films. *Journal of Polymer Science Part B: Polymer Physics*, **39**, 2923–2936 (2001).
<https://doi.org/10.1002/polb.10049>
- [11] Kojima M., Magill J., Lin J., Magonov S.: Structure and morphology of biaxially oriented films of polyethylenes. *Chemistry of Materials*, **9**, 1145–1153 (1997).
<https://doi.org/10.1021/cm960505h>

- [12] Larena A., Pinto G.: The effect of surface roughness and crystallinity on the light scattering of polyethylene tubular blown films. *Polymer Engineering and Science*, **33**, 742–747 (1993).
<https://doi.org/10.1002/pen.760331204>
- [13] Zhao H., Zhang Q., Li L., Chen W., Wang D., Meng L., Li L.: Synergistic and competitive effects of temperature and flow on crystallization of polyethylene during film blowing. *ACS Applied Polymer Materials*, **1**, 1590–1603 (2019).
<https://doi.org/10.1021/acsapm.9b00391>
- [14] Troisi E., van Drongelen M., Caelers H., Portale G., Peters G.: Structure evolution during film blowing: An experimental study using *in-situ* small angle X-ray scattering. *European Polymer Journal*, **74**, 190–208 (2016).
<https://doi.org/10.1016/j.eurpolymj.2015.11.022>
- [15] Throne J. L.: Understanding thermoforming. Hanser, Cincinnati (2008).
- [16] Auinger T., Stadlbauer M.: Inter-relationship between processing conditions and mechanical properties of blown film from different polypropylenes and high melt strength polypropylene blends. *Journal of Applied Polymer Science*, **117**, 155–162 (2010).
<https://doi.org/10.1002/app.31928>
- [17] Hoenic W., Bosnyak C., Sehanobish K., van Volkenburgh W., Ruiz C., Tau L.: New polypropylene for differentiated blown films. in ‘ANTEC 2000 Conference proceedings, Orlando, Florida’ 1843–1846 (2000).
- [18] Münstedt H., Kurzbeck S., Stange J.: Advances in film blowing, thermoforming, and foaming by using long-chain branched polymers. *Macromolecular Symposia*, **245**, 181–190 (2006).
<https://doi.org/10.1002/masy.200651326>
- [19] Chang A. C., Tau L., Hiltner A., Baer E.: Structure of blown film from blends of polyethylene and high melt strength polypropylene. *Polymer*, **43**, 4923–4933 (2002).
[https://doi.org/10.1016/S0032-3861\(02\)00304-X](https://doi.org/10.1016/S0032-3861(02)00304-X)
- [20] Lau H., Bhattacharya S., Field G.: Melt strength of polypropylene: Its relevance to thermoforming. *Polymer Engineering and Science*, **38**, 1915–1923 (1998).
<https://doi.org/10.1002/pen.10362>
- [21] Silva J., Elias M., Lima N., Canevarolo S.: Morphology in multilayer blown films of polypropylene and ethylene-octene copolymer blends. *International Polymer Processing*, **33**, 345–354 (2018).
<https://doi.org/10.3139/217.3526>
- [22] Zhang X. M., Ajji A.: Oriented structure of PP/LLDPE multilayer and blends films. *Polymer*, **46**, 3385–3393 (2005).
<https://doi.org/10.1016/j.polymer.2005.03.004>
- [23] Bheda J. H., Spruiell J. E.: The effect of process and polymer variables on the light transmission properties of polypropylene tubular blown films. *Polymer Engineering and Science*, **26**, 736–745 (1986).
<https://doi.org/10.1002/pen.760261105>
- [24] Natta G., Corradini P.: Structure and properties of isotactic polypropylene. in ‘Stereoregular polymers and stereospecific polymerizations’ (eds.: Natta G., Danusso F.) Elsevier, Amsterdam, 743–746 (1967).
- [25] Carmeli E., Cavallo D., Tranchida D.: Instrument for mimicking fast cooling conditions of polymers: Design and case studies on polypropylene. *Polymer Testing*, **97**, 107164 (2021).
<https://doi.org/10.1016/j.polymertesting.2021.107164>
- [26] di Sacco F., Gahleitner M., Wang J., Portale G.: Systematic investigation on the structure-property relationship in isotactic polypropylene films processed *via* cast film extrusion. *Polymers*, **12**, 1636 (2020).
<https://doi.org/10.3390/polym12081636>
- [27] Xu M., Zhang S., Liang J., Quan H., Liu J., Shi H., Gao D., Liu J.: Influences of processing on the phase transition and crystallization of polypropylene cast films. *Journal of Applied Polymer Science*, **131**, 41100 (2014).
<https://doi.org/10.1002/app.41100>
- [28] di Sacco F., Solano E., Malfois M., Wang J., Gahleitner M., Pantani R., Portale G.: Real-time structural characterization of isotactic polypropylene during cast film extrusion. *Polymer*, **276**, 125914 (2023).
<https://doi.org/10.1016/j.polymer.2023.125914>
- [29] Savolainen A.: Biaxially oriented polypropylene blown films. I: Morphological analysis of orientation in the machine direction. *Polymer Engineering and Science*, **30**, 1258–1264 (1990).
<https://doi.org/10.1002/pen.760301910>
- [30] Shanks R. A., Li J., Yu L.: Polypropylene–polyethylene blend morphology controlled by time–temperature–miscibility. *Polymer*, **41**, 2133–2139 (2000).
[https://doi.org/10.1016/S0032-3861\(99\)00399-7](https://doi.org/10.1016/S0032-3861(99)00399-7)
- [31] Svoboda P., Svobodova D., Slobodian P., Ougizawa T., Inoue T.: Transmission electron microscopy study of phase morphology in polypropylene/ethylene-octene copolymer blends. *European Polymer Journal*, **45**, 1485–1492 (2009).
<https://doi.org/10.1016/j.eurpolymj.2009.01.032>
- [32] Greso A. J., Phillips P. J.: The role of secondary nucleation in epitaxial growth: The template model. *Polymer*, **35**, 3373–3376 (1994).
[https://doi.org/10.1016/0032-3861\(94\)90897-4](https://doi.org/10.1016/0032-3861(94)90897-4)
- [33] Paulik C., Tranninger C., Wang J., Shutov P., Mileva D., Gahleitner M.: Catalyst type effects on structure/property relations of polypropylene random copolymers. *Macromolecular Chemistry and Physics*, **222**, 2100302 (2021).
<https://doi.org/10.1002/macp.202100302>
- [34] Mileva D., Wang J., Androsch R., Jariyavidyanont K., Gahleitner M., Bernreitner K.: Crystallization of random metallocene-catalyzed propylene-based copolymers with ethylene and 1-hexene on rapid cooling. *Polymers*, **13**, 2091 (2021).
<https://doi.org/10.3390/polym13132091>

- [35] Menyhárd A., Gahleitner M., Varga J., Bernreitner K., Jääskeläinen P., Øysæd H., Pukánszky B.: The influence of nucleus density on optical properties in nucleated isotactic polypropylene. *European Polymer Journal*, **45**, 3138–3148 (2009).
<https://doi.org/10.1016/j.eurpolymj.2009.08.006>
- [36] Wang W.-J., Zhu S.: Structural analysis of ethylene/propylene copolymers synthesized with a constrained geometry catalyst. *Macromolecules*, **33**, 1157–1162 (2000).
<https://doi.org/10.1021/ma991614v>
- [37] Tzoganakis C., Vlachopoulos J., Hamielec A. E., Shinozaki D. M.: Effect of molecular weight distribution on the rheological and mechanical properties of polypropylene. *Polymer Engineering and Science*, **29**, 390–396 (1989).
<https://doi.org/10.1002/pen.760290607>
- [38] Bremner T., Rudin A., Cook D. G.: Melt flow index values and molecular weight distributions of commercial thermoplastics. *Journal of Applied Polymer Science*, **41**, 1617–1627 (1990).
<https://doi.org/10.1002/app.1990.070410721>
- [39] Winter H. H.: Three views of viscoelasticity for Cox–Merz materials. *Rheologica Acta*, **48**, 241–243 (2009).
<https://doi.org/10.1007/s00397-008-0329-5>
- [40] Rathinaraj J. D. J., Keshavarz B., McKinley G. H.: Why the Cox–Merz rule and Gleissle mirror relation work: A quantitative analysis using the Wagner integral framework with a fractional Maxwell kernel. *Physics of Fluids*, **34**, 033106 (2022).
<https://doi.org/10.1063/5.0084478>
- [41] Tranchida D., Resconi L.: Influence of 2,1-erythro regiodefects on the crystallization behavior of isotactic polypropylene. *Polymer Crystallization*, **1**, e10022 (2018).
<https://doi.org/10.1002/pcr2.10022>
- [42] Pae K. D.: γ – α Solid–solid transition of isotactic polypropylene. *Journal of Polymer Science A-2: Polymer Physics*, **6**, 657–663 (1968).
<https://doi.org/10.1002/pol.1968.160060401>
- [43] Thomann R., Wang C., Kressler J., Mülhaupt R.: On the γ -phase of isotactic polypropylene. *Macromolecules*, **29**, 8425–8434 (1996).
<https://doi.org/10.1021/ma951885f>
- [44] Foresta T., Piccarolo S., Goldbeck-Wood G.: Competition between α and γ phases in isotactic polypropylene: Effects of ethylene content and nucleating agents at different cooling rates. *Polymer*, **42**, 1167–1176 (2001).
[https://doi.org/10.1016/S0032-3861\(00\)00404-3](https://doi.org/10.1016/S0032-3861(00)00404-3)
- [45] Obadal M., Čermák R., Stoklasa K.: Tailoring of three-phase crystalline systems in isotactic poly(propylene). *Macromolecular Rapid Communications*, **26**, 1253–1257 (2005).
<https://doi.org/10.1002/marc.200500272>
- [46] Sajkiewicz P., Grady A., Ziabicki A., Misztal-Faraj B.: On the metastability of β phase in isotactic polypropylene: Experiments and numerical simulation. *e-Polymers*, **10**, 124 (2010).
<https://doi.org/10.1515/epoly.2010.10.1.1398>
- [47] Tan D. Q., Liu Y., Lin X., Huang E., Lin X., Wu X., Lin J., Luo R., Wang T.: Exploration of breakdown strength decrease and mitigation of ultrathin polypropylene. *Polymers*, **15**, 2257 (2023).
<https://doi.org/10.3390/polym15102257>
- [48] Wong A. C-Y.: Splitting characteristics of polyethylene films. *Journal of Materials Processing Technology*, **38**, 63–69 (1993).
[https://doi.org/10.1016/0924-0136\(93\)90186-A](https://doi.org/10.1016/0924-0136(93)90186-A)
- [49] Kim Y.-M., Kim C.-H., Park J.-K., Lee C.-W., Min T.-I.: Morphological considerations on the mechanical properties of blown high-density polyethylene films. *Journal of Applied Polymer Science*, **63**, 289–299 (1997).
[https://doi.org/10.1002/\(SICI\)1097-4628\(19970118\)63:3<289::AID-APP3>3.0.CO;2-J](https://doi.org/10.1002/(SICI)1097-4628(19970118)63:3<289::AID-APP3>3.0.CO;2-J)
- [50] Resch K., Wallner G. M., Teichert C., Gahleitner M.: Highly transparent polypropylene cast films: Relationships between optical properties, additives, and surface structure. *Polymer Engineering and Science*, **47**, 1021–1032 (2007).
<https://doi.org/10.1002/pen.20781>
- [51] Mileva D., Gahleitner M., Gloger D., Tranchida D.: Crystal structure: A way to control properties in cast films of polypropylene. *Polymer Bulletin*, **75**, 5587–5598 (2018).
<https://doi.org/10.1007/s00289-018-2343-9>